Precision Engineering 56 (2019) 485–495

Contents lists available at ScienceDirect

Precision Engineering

journal homepage: www.elsevier.com/locate/precision

On the validity of compliance-based matrix method in output compliance modeling of flexure-hinge mechanism

Jianjian Wang[a,b], Yang Yang[a], Ru Yang[c], Pingfa Feng[d], Ping Guo[c,*]

[a] Department of Mechanical and Automation Engineering, Chinese University of Hong Kong, China
[b] Shun Hing Institute of Advanced Engineering, Chinese University of Hong Kong, China
[c] Department of Mechanical Engineering, Northwestern University, Evanston, IL, USA
[d] Department of Mechanical Engineering, Tsinghua University, China

ARTICLE INFO

Keywords:
Flexure hinge mechanism
Right circular flexure hinge
Compliance-based matrix method
Output compliance
Parallel mechanism
Ill-condition

ABSTRACT

Compliance-based matrix method (CMM) has been regarded as an efficient technique for output compliance modeling of the flexure hinge-based compliant mechanism, owing to its simplicity and high accuracy. However, this study demonstrates that CMM is not always valid due to the intrinsic ill-condition of the compliance matrix of right circular flexure hinge (RCFH). Inversion of compliance matrix can result in numerical instability in the calculation of its stiffness matrix. It is shown in this study that CMM can be effectively applied to serial compliant mechanism, while its adoption in modeling parallel compliant mechanism needs to be carefully examined due to the matrix inversion involved. The validity of CMM is highly dependent on the spatial configuration, degree of freedom, and singularity of the parallel mechanism. The validity criteria of CMM are discussed in detail with exemplary configurations of 3RRR, 2RR, and bridge-type compliant mechanisms.

1. Introduction

Flexure-hinge mechanisms are composed of rigid links and flexure hinges, which are capable of transmitting smooth micro motions through the elastic deformation of flexure hinges [1]. Due to their unique and superior motion transmission properties including zero backlash, zero friction, and low wear, compliant mechanism designs have emerged as a promising and reliable technique for precision engineering applications, such as vibration cutting tools [2,3], scanning electron and atomic force microscopy, micro assembly, nanoimprint lithography [4], biological cell micro-injection [5,6], etc.

Modeling the deformation of compliant mechanism, including kinematic, static, and dynamic behaviors, is vital for its structure analysis and dimension synthesis during the design stage. Output compliance (inverse of stiffness), which characterizes the relationship between the applied loads on the output platform and its deformation, is one of the most important performance index that needs to be accurately modeled. For example, the output compliance of a vibration cutting tool composed of compliant mechanism is critical for determining its cutting performance and stability.

Analytical modeling and finite element method (FEM) are the two most commonly used techniques in output compliance modeling. Due to its high accuracy and flexibility, FEM is usually regarded as a reliable method to model complex structure dynamics. It, however, cannot establish the analytical relationship between the output compliance and the dimensions and spatial configurations of compliant mechanism [7]. Consequently, FEM is appropriate as a tool to verify the performance of compliant mechanism once the specific dimension and spatial configuration have already been determined [7]. More often, FEM is utilized for the comparison among different analytical modeling methods rather than for the dimension synthesis of compliant mechanism. Analytical modeling approaches, on the other hand, are preferred for the dimension synthesis of compliant mechanism. Among various analytical modeling methods including the pseudo-rigid-body method [8] and Castigliano's theorem [9], compliance-based matrix method (CMM) can be regarded as a reduced FEM [5]. Compared to the pseudo-rigid-body method, the matrix method is capable of complete compliance analysis since it considers the flexure compliances in all working degrees of freedom [10].

Due to its simplicity and capability of modeling complex structures, CMM has been widely utilized in modeling of various compliant mechanisms. Pham and Chen developed a general modeling approach based on CMM for compliance modeling of flexure mechanisms, and successfully applied the model to a double linear spring and a three degree-of-freedom (DOF) translational parallel mechanisms with FEM and experiment verification [7]. Choi and Lee derived a static model

* Corresponding author.
E-mail address: ping.guo@northwestern.edu (P. Guo).

https://doi.org/10.1016/j.precisioneng.2019.02.006
Received 18 October 2018; Received in revised form 3 January 2019; Accepted 6 February 2019
Available online 12 February 2019

Nomenclature[1]

CMM	compliance-based matrix method
RCFH	right circular flexure hinge
R	radius of RCFH
t	neck thickness of RCFH
b	thickness of RCFH
$\Delta\alpha$	rotational motion about the z-axis
Δy	translational motion in the y-axis
Δx	translational motion in the x-axis
M_z	rotational motions about the z-axis
F_x	force in the y-axis
F_y	force in the x-axis
$\mathbf{C}_{\mathrm{RCFH}}$	compliance matrix of RCFH
$\mathbf{K}_{\mathrm{RCFH}}$	stiffness matrix of RCFH
C_{ij}	compliance factor in ith row and jth column of $\mathbf{C}_{\mathrm{RCFH}}$
K_{ij}	stiffness factor in ith row and jth column of $\mathbf{K}_{\mathrm{RCFH}}$
$\mathbf{C}_{\mathrm{serial}}$	compliance matrix of serial compliant mechanism
$\mathbf{C}_{\mathrm{parallel}}$	compliance matrix of parallel compliant mechanism
$C_{\mathrm{name},ij}$	the element at the ith row and jth column of $\mathbf{C}_{\mathrm{name}}$; 'name' can be substituted by the particular compliant mechanism name, such as serial, parallel, bridge, 3RRR, 2RR, etc.
$\mathbf{T}_i^0$	transformation matrix from frame $x_iO_iy_i$ to reference frame xOy which is attached to the output platform
$\mathbf{T}_j^i$	transformation matrix from frame $x_jO_jy_j$ to reference frame $x_iO_iy_i$
E	elastic modulus of RCFH material
v	Poisson's ratio of RCFH material

using CMM for a flexure-based mechanism driven by piezo actuators [11]. Lobontiu utilized the matrix method to model the direct and inverse quasi-static response of constrained/over-constrained planar mechanisms, the results of which were verified by FEM [12]. Jia et al. developed a 3-DOF positioning stage for nanoimprint lithography, and modeled the stiffness of compliant mechanism using CMM [4]. Yong and Lu employed the matrix method to conduct kinetostatic modeling of a 3-RRR compliant micro-motion stage composed of flexure hinges [6]. Zhu et al. developed a 2-D vibration cutting tool using flexure mechanism, and adopted CMM to construct the tool-tip compliance matrix [2]. They also presented an optimized design of a piezo-actuated multi-axial compliant structure for micro-/nano-cutting with the help of CMM [13,14].

The modeling accuracy of the overall output compliance of parallel mechanism using CMM strongly depends on the modeling accuracy of individual right circular flexure hinge (RCFH) [15]. Various methods including inverse conformal mapping [16], Castigliano's second theorem [17], and the integration of linear differential equations of beams [18], have been used to estimate the compliance matrix of flexure hinges. Yong et al. [15] compared the calculated compliance from various analytical models for circular flexure hinges with the FEM results, including the equations developed by Paros and Weisbord [18], Lobontiu [19], Wu and Zhou [20], Tseytlin [16], Smith et al. [21] and Schotborgh et al. [22]. According to their results, the accuracy of these compliance equations is inconsistent at different radius R to neck thickness t ratios (see Fig. 1 for hinge geometries). In certain circumstances, the calculation errors would even be as high as 40%. They also assessed the estimation accuracy of compliance matrix of RCFH on the output compliance of a particular 3RRR mechanism [6]. However, the assessment in their research was performed just for a particular instance without considering the influence of different spatial configurations. The spatial configuration of compliant mechanism determines the motion and force transmission between input and output pairs, which has a decisive impact on the modeling accuracy and validity of the matrix method. The relationship between the spatial configuration and modeling accuracy has not been well investigated in previous research. As this study is to show, the matrix method is indeed not always valid in many cases.

This study presents the validity assessment of CMM in the output compliance modeling of flexure-hinge mechanism, particularly in an attempt to answer the question that how the spatial configuration affects the validity of the matrix method. Firstly, the intrinsic ill-condition of compliance matrix expressed in its local coordinate frame of RCFH is discovered. The effect of compliance accuracy on the calculation error of stiffness factors for RCFH by matrix inversion is derived. Then the effect of matrix ill-condition on the modeling accuracy of output compliance for both serial and parallel compliant mechanisms is analyzed. The 3RRR, 2RR and bridge-type compliant mechanisms are taken as calculation examples to evaluate the validity of CMM. A general criterion is proposed to determine whether the matrix method is valid for output compliance modeling of flexure mechanism, with consideration of the mechanism type (serial or parallel), spatial configuration, degree of freedom, and mechanism singularity.

2. Theoretical analysis on validity of CMM

2.1. Intrinsic ill-condition of compliance matrix of RCFH

As shown in Fig. 1(c), the compliance matrix $\mathbf{C}_{\mathrm{RCFH}}$ of a RCFH in its local coordinate system represents the compliance of free end O_i with respect to the other fixed end. It can be expressed as a 3 × 3 matrix as:

$$\mathbf{C}_{\mathrm{RCFH}} = \begin{bmatrix} C_{11} & 0 & 0 \\ 0 & C_{22} & C_{23} \\ 0 & C_{32} & C_{33} \end{bmatrix} = \begin{bmatrix} \frac{\Delta x}{F_x} & 0 & 0 \\ 0 & \frac{\Delta y}{F_y} & \frac{\Delta y}{M_\alpha} \\ 0 & \frac{\Delta \alpha}{F_y} & \frac{\Delta \alpha}{M_z} \end{bmatrix} \tag{1}$$

The compliance factors C_{ij} (i,j = 1,2,3) in the matrix can be derived as a function of geometric parameters and material properties of RCFH [15], namely $C_{ij} = f_{ij}(R, t, b, E, \upsilon)$. Due to the coupled deformations of a RCFH, the compliance factors C_{ij} are not all mutually independent. Actually, C_{23} and C_{32} depend on C_{33}, namely $C_{23} = C_{32} = C_{33}R$ [15]. Among the five compliance factors, only $C_{11} = \Delta x/F_x$, $C_{22} = \Delta y/F_y$, and $C_{33} = \Delta\alpha/M_z$ are independent variables that can be calculated following the derivations shown in Appendix A.

Theoretically, the stiffness matrix $\mathbf{K}_{\mathrm{RCFH}}$ of RCFH can be derived by inversing the compliance matrix $\mathbf{C}_{\mathrm{RCFH}}$:

$$\mathbf{K}_{\mathrm{RCFH}} = \mathbf{C}_{\mathrm{RCFH}}^{-1} = \begin{bmatrix} K_{11} & 0 & 0 \\ 0 & K_{22} & K_{23} \\ 0 & K_{32} & K_{33} \end{bmatrix} \tag{2}$$

where K_{ij} (i,j = 1,2,3) are the stiffness factors of $\mathbf{K}_{\mathrm{RCFH}}$, which can be calculated according to the equations derived in Appendix A.

However, based on the matrix theory, matrix inversion should be carefully carried out due to its potential instability [23]. If a matrix is ill-conditioned, a tiny variation of its element would induce huge variations in its inverse. The matrix inversion can result in unacceptable calculation errors leading to the large deviation of stiffness matrix estimation in actual engineering application. In Eq. (1), the compliance factors of RCFH obtained by analytical calculation or FEM are not always accurate with respect to their true values [15]. In some circumstances, the calculation errors of these equations of RCFH compliances would be as high as 40% [15]. Hence, the inverse operation of $\mathbf{C}_{\mathrm{RCFH}}$ as illustrated in Eq. (2) should always be carefully carried out as demonstrated in the following examples.

[1] Note: Vectors and matrices are shown in bold face

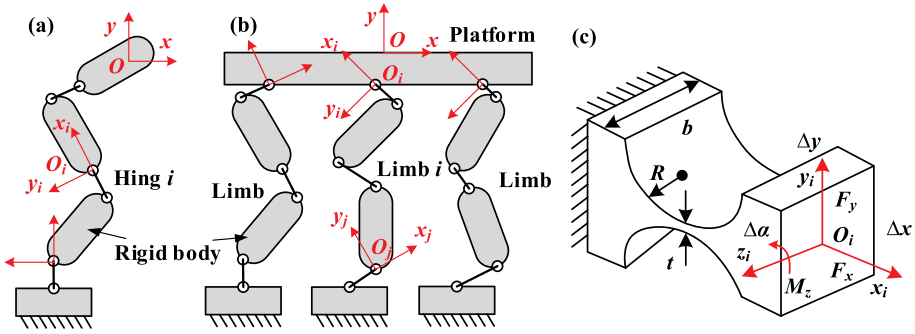

Fig. 1. Flexure hinge-based compliant mechanism of (a) serial and (b) parallel types; and (c) coordinate system of a right circular flexure hinge (RCFH).

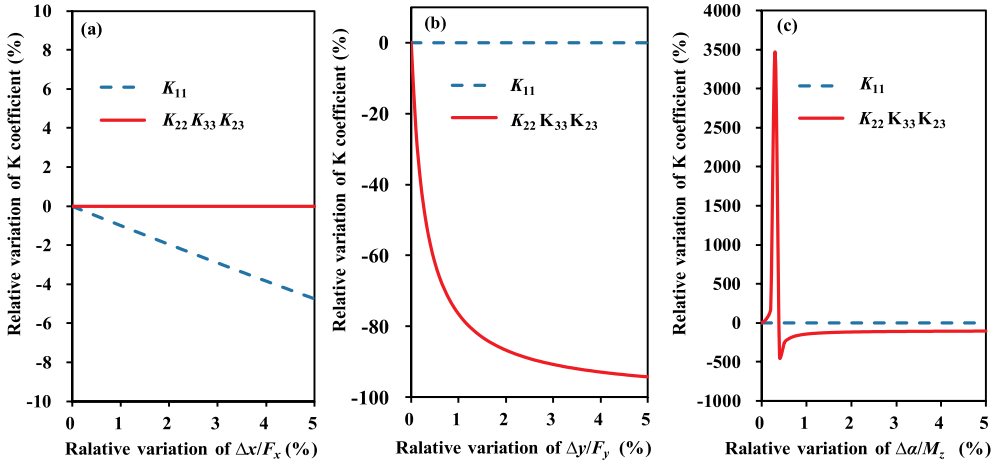

Fig. 2. Effect of compliance variation of RCFH on the stiffness variation of RCFH obtained by matrix inversion.

Fig. 2 shows the effects of compliance variation of RCFH on the stiffness variation of RCFH obtained by matrix inversion, where $E = 210$ GPa, $\nu = 0.3$, $R = 1$ mm, $t = 0.5$ mm, and $b = 5$ mm. As shown in Fig. 2(a), the variation of K_{11} is linearly related to the variation of $\Delta x/F_x$. That is to say if the variation of $\Delta x/F_x$ is tiny, the variation of K_{11} is also small. The variation of $\Delta y/F_y$ and $\Delta\alpha/M_z$, on the other hand, can induce extremely large variations of K_{22}, K_{23} and K_{33}. When the relative variation of $\Delta y/F_y$ reaches only 1%, the relative variation of K_{22}, K_{23} and K_{33} can exceed 80%. When the relative variation of $\Delta\alpha/M_z$ is only 0.3%, the relative variation of K_{22}, K_{23} and K_{33} can even reach up to 3500%. These results indicate that the compliance matrix $\mathbf{C}_{\mathrm{RCFH}}$ of RCFH is extremely ill-conditioned. $\mathbf{C}_{\mathrm{RCFH}}$ is usually ill-conditioned due to the specific structure of RCFH. The rotational compliance of RCFH is much larger than the compliances in other directions, making the different elements of $\mathbf{C}_{\mathrm{RCFH}}$ vary in magnitudes. A tiny calculation error of $\Delta y/F_y$ and $\Delta\alpha/M_z$ with respect to their true values would induce unacceptably large calculation error of stiffness factors. Fig. 2 also indicates that the ill-condition of RCFH compliance matrix is highly related to the tangential translational compliance ($\Delta y/F_y$) and rotational compliance ($\Delta\alpha/M_z$).

Though the analysis above is based on the compliance equations of RCFH, which is a particular type of notch flexures [24,25], the conclusions are also applicable to most types of flexure designs. For example, the compliance factors of general notch flexures are usually not well balanced due their specific design for enhancing the rotational degree of freedom. The rotational compliance of notch flexures is much larger than the compliances in other directions, making the matrices ill-conditioned as well. Moreover, the compliance matrix of leaf spring flexure hinge, which has straight beams of uniform cross-sections, is also ill-conditioned based on the same principle above. It is also worthy to note that the inversion problem cannot be easily overcome by using the stiffness matrix. The stiffness matrix is usually obtained from the inversion of compliance matrix since it is more difficult to derive the stiffness matrix elements by their direct definition. In addition, if the compliance matrix is ill conditioned, the stiffness matrix will be also ill conditioned, because they share the same condition number with each other [23].

2.2. Validity evaluation method of CMM for the output compliance modeling of flexure mechanism

For compliant mechanism composed of serially and parallelly connected RCFHs, the calculation error of compliance matrix of RCFHs is accumulated and added to the final modeling error of the overall output compliance. The validity of CMM is established based on the insensitivity of the output compliance variation on the variation of compliance factors of individual RCFHs.

As shown in Fig. 1, the compliant mechanism can be classified into two categories, namely the serial and the parallel compliant mechanisms. The output compliances of these two types can be expressed by:

$$\begin{cases} \mathbf{C}_{\mathrm{serial}} = \sum \mathbf{T}_i^0 \mathbf{C}_{\mathrm{RCFH}} (\mathbf{T}_i^0)^{\mathrm{T}} \\ \mathbf{C}_{\mathrm{parallel}} = \left(\sum_i \left(\mathbf{T}_i^0 \left(\sum_j \mathbf{T}_j^i \mathbf{C}_{\mathrm{RCFH}} (\mathbf{T}_j^i)^{\mathrm{T}} \right) (\mathbf{T}_i^0)^{\mathrm{T}} \right)^{-1} \right)^{-1} \end{cases} \tag{3}$$

where $\mathbf{C}_{\mathrm{serial}}$ and $\mathbf{C}_{\mathrm{parallel}}$ represent the output compliance matrices of serial and parallel flexure mechanisms respectively. Detailed derivation of Eq. (3) and expressions of transformation matrices can be found in Appendix B.

According to Eq. (3), the compliance factor $C_{\mathrm{serial},ij}$ of $\mathbf{C}_{\mathrm{serial}}$ can be derived as:

$$C_{\mathrm{serial},ij} = \lambda_{ij}^{11} C_{11} + \lambda_{ij}^{22} C_{22} + \lambda_{ij}^{33} C_{33} \tag{4}$$

where $C_{serial,ij}$ is the compliance factor at the ith row and jth column of the matrix $\mathbf{C}_{serial}$; λ_{ij}^{11}, λ_{ij}^{22}, and λ_{ij}^{33} are the corresponding coefficients of RCFH compliances. As illustrated by Eq. (4), the output compliances of serial flexure mechanism are the linear superposition of RCFH compliance factors without introducing any matrix inversion operation. The calculation errors thus are bounded given that the RCFH compliances are calculated with acceptable accuracy.

However, as illustrated in Eq. (3), the inversion of compliance matrix is always required to calculate the output compliance matrix $\mathbf{C}_{parallel}$ of parallel flexure mechanism. Because of its indispensable matrix inverse operation, the calculation error of output compliance of parallel flexure mechanism might be extremely large due to the ill-condition of individual compliance matrix as demonstrated in section 2.1. In order to evaluate the validity of the matrix method in the output compliance modeling of parallel flexure mechanism, the effects of the variation of individual RCFH compliance factors on the accuracy of final output compliance are assessed based on the following equation:

$$\Delta C_{parallel,ij} = \left| \frac{\delta C_{parallel,ij}}{C_{parallel,ij}} \right| \tag{5}$$

where $\Delta C_{parallel,ij}$ donates the relative variation of calculated output compliance due to the compliance variation of RCFH induced by modeling error. The variation of output compliance $\delta C_{parallel,ij}$ is calculated based on the following rules. When the effect of one compliance factor C_{ij} (such as C_{11}) is to be evaluated, the variation is set to 5%, while keeping the other two compliance factors (such as C_{22}, C_{33}) unchanged.

Based on the above analysis of Eq. (3), the matrix method is always valid in the output compliance modeling for serial flexure mechanism. Therefore, this study focuses on the validity evaluation of CMM for parallel flexure mechanism. The evaluation results for typical parallel mechanisms including 3RRR, 2RR and bridge-type are demonstrated in section 3.

2.3. Validity condition of CMM for output compliance modeling of parallel flexure mechanism

The potential invalidity of CMM results from the ill-condition of compliance matrix of RCFH and the matrix inversion operations during calculation. The compliance matrix of RCFH is usually ill-conditioned; however, the matrix method has still been successfully utilized for analysis of many kinds of parallel flexure mechanisms as illustrated in the introduction. The accuracy of overall output compliance is not only influenced by the inversion error due to the matrix ill-condition, but also related to the spatial configuration of parallel mechanism. It turns out that the inversion error can be bounded if certain configuration conditions are met even with the ill-conditioned compliance matrices of individual RCFHs.

The ill-condition of compliance matrix is highly related to the relative magnitudes between the translational compliance and rotational compliance (as illustrated by Eq. (A. 4) in Appendix A). Only if the radial translational compliance $\Delta x/F_x$ or the rotational compliance $\Delta\alpha/M_z$ of RCFH is dominant in the output compliance of parallel flexure mechanism, the CMM is valid. We further examine this hypothesis by simplifying the RCFH as a revolute pair with only the rotational DOF. The overall DOF of any parallel flexure mechanism then can be determined according to the DOF analysis theory of parallel mechanism [26]. When the spatial configuration of parallel mechanism is singular, rotational compliance of RCFH may lose its dominance. At this time, the dominance of radial translational compliance of RCFH should also be checked to determine the validity of the matrix method. If none of the radial translational or rotational compliance is dominant, the CMM will be invalid for output compliance modeling.

Although the above validity criteria of CMM cannot be described by a set of mathematical equations, they provide a general evaluation method to determine the validity of CMM for parallel flexure-hinge mechanism with various spatial configurations. Detailed examples are given below based on 3RR, 2RR, and bridge-type mechanisms to demonstrate the validity of the proposed criteria.

3. Case study of CMM validity

Fig. 3 shows the specific spatial configurations of typical 3RRR, 2RR and bridge-type mechanisms, where D_M, D_x and D_y represent the rotational and translational DOFs along the corresponding axes. The DOF analysis for the above parallel mechanisms will be conducted for validity evaluation of CMM.

3.1. 3RRR compliant mechanism

The spatial configuration of 3RRR compliant mechanism is

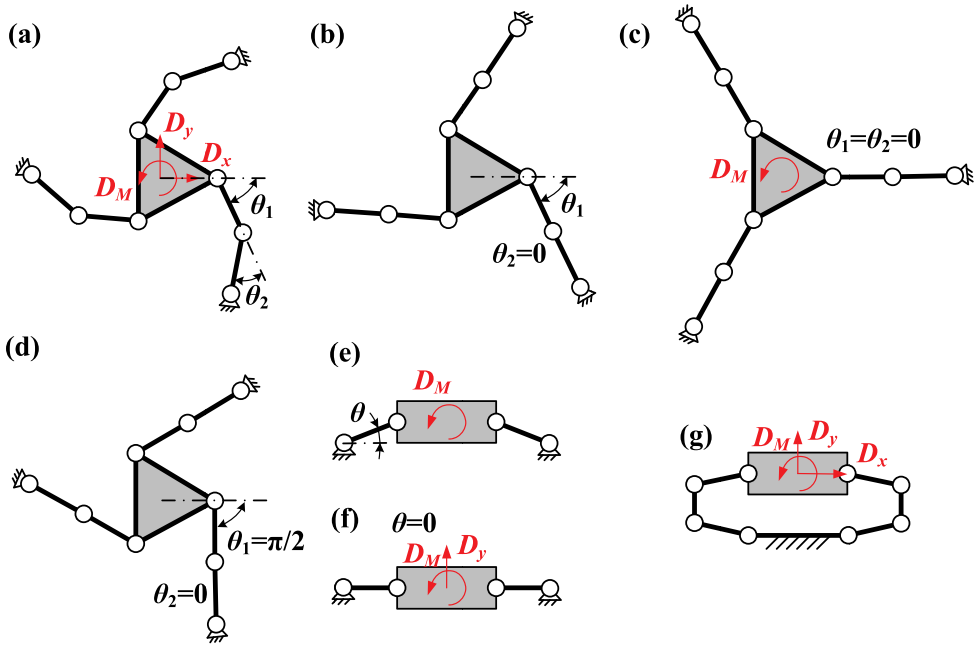

Fig. 3. DOF analysis of 3RRR, 2RR and bridge-type mechanisms: 3RRR with (a) $0 < |\theta_1| < \pi/2$ and $0 < |\theta_2| < \pi/2$, (b) $0 < |\theta_1| < \pi/2$ and $\theta_2 = 0$, (c) $\theta_1 = \theta_2 = 0$, and (d) $\theta_1 = \pi/2$ and $\theta_2 = 0$; 2RR with (e) $\theta \neq 0$ and (f) $\theta = 0$; and (g) bridge-type mechanism.

illustrated in Fig. 4, where θ_1 and θ_2 are the relative rotation angles of adjacent arms. It consists of three RRR chains connected together in parallel, while each chain is composed of three RCFHs. Due to the central symmetry of 3RRR compliant mechanism, it has the characteristic of compliance decoupling. Based on compliance-based matrix modeling, the output compliance matrix $\mathbf{C}_{3RRR}$ of 3RRR compliant mechanism can be derived as:

$$\mathbf{C}_{3RRR} = \begin{bmatrix} C_{3RRR,tran} & 0 & 0 \\ 0 & C_{3RRR,tran} & 0 \\ 0 & 0 & C_{3RRR,rota} \end{bmatrix} \tag{6}$$

where $C_{3RRR,tran}$ and $C_{3RRR,rota}$ denote the translational compliance and rotational compliance of 3RRR compliant mechanism respectively. Detailed derivation of Eq. (6) is illustrated in Appendix C.1. Fig. 4(c) shows the FEM model for calculating the output compliance of 3RRR compliant mechanism. The FEM results are taken as the reference values when evaluating the accuracy of CMM results in different cases.

Fig. 5 shows the contour plots of output compliance variation of 3RRR compliant mechanism due to the compliance variance of $\Delta x/F_x$ and $\Delta\alpha/M_z$ under different spatial configurations (θ_1 and θ_2). The variations of $\Delta x/F_x$ and $\Delta\alpha/M_z$ are assumed to be both 5%. As shown in Fig. 5(a) and (b), the output compliance variations are always smaller than 5% regardless the spatial configuration of the system. On the other hand, the variation of $\Delta\alpha/M_z$ triggers the numerical instability when calculating the output rotational compliance $C_{3RRR,rota}$. As demonstrated in Fig. 5(c) and (d), the relative variation of calculated rotational compliance $C_{3RRR,rota}$ reaches 800% when the spatial angles θ_1 and θ_2 equal to $\pi/4$ and 0 respectively. It indicates that CMM is only valid for modeling 3RRR under certain spatial configurations. This validity dependency is further discussed as follows.

(1) Fig. 3(a) shows a general spatial configuration of 3RRR mechanism where $\theta_2 \neq 0$ and $0 < |\theta_1| < \pi/2$. This spatial configuration has three DOFs and is away from the singular point. Under such condition, the rotational compliance of RCFH is dominant in the output compliances of 3RRR mechanism. The CMM can be well utilized in the output compliance modeling of 3RRR compliant mechanism. In order to verify the dominance of rotational compliance, the calculation accuracy of the matrix method is evaluated and compared with FEM results including two cases. The first case includes all the translational and rotational compliances of 3RRR mechanism. The second case contains only the rotational compliance, considering the dominance of its influence. The specific calculation conditions of these two cases are listed in Table 1. The calculation results are demonstrated in Table 2.

As the verification results shown in Table 2, for the general 3RRR compliant mechanism away from the singular configuration, the calculation accuracy of CMM is acceptable, even if the individual compliance matrix of RCFH is ill-conditioned. Furthermore, when the compliance factors including $\Delta x/F_x$ or $\Delta y/F_y$ is neglected in Case 2, the calculation results of the matrix method do not vary significantly compared with the results shown in Case 1. This result verifies the dominance of rotational compliance of RCFH in the output compliance of 3RRR compliant mechanism for the general spatial configuration shown in Fig. 3(a).

(2) Fig. 3(b) shows a specific spatial configuration of 3RRR mechanism where $\theta_2 = 0$ and $0 < |\theta_1| < \pi/2$. This spatial configuration has zero DOF and is singular. Neither the rotational or radial translational compliance of RCFH is dominant in the output compliances of 3RRR mechanism. The CMM is not suitable to be utilized in its output compliance modeling of 3RRR mechanism for the spatial configuration in Fig. 3(b). As shown in Fig. 5(c) and (d), in this configuration, the relative variations resulting from the tiny variation of RCFH compliance are extremely large, which indicates the invalidity of the matrix method.

(3) Fig. 3(c) shows a specific spatial configuration of 3RRR mechanism where $\theta_1 = \theta_2 = 0$. This spatial configuration is also singular. However, since the extended lines of three limbs intersect at the same point, it has one rotational DOF. The rotational compliance of RCFH is dominant in the output rotational compliance of 3RRR mechanism, while the radial translational compliance of RCFH is dominant in the output translational compliance of 3RRR mechanism. As shown in Fig. 5, consistent with the above analysis, when the rotational compliance or the radial translational compliance is dominant, the matrix method can be utilized in the output modeling of the 3RRR spatial configuration of Fig. 3(c) with acceptable accuracy.

(4) Fig. 3(d) shows a special spatial configuration of 3RRR mechanism where $\theta_2 = 0$ and $\theta_1 = \pi/2$. This spatial configuration has zero DOF and is singular. However, the radial translational compliance of RCFH is dominant in the output compliances of 3RRR compliant mechanism as shown in Fig. 5. The CMM can also be well utilized in for the case in Fig. 3(d).

3.2. 2RR compliant mechanism

The spatial configuration of parallel 2RR mechanisms is illustrated in Fig. 6. It consists of two RR chains connected together in parallel. Each chain is composed of two RCFHs. Based on CMM, the output compliance matrix $\mathbf{C}_{2RR}$ of 2RR mechanism can be derived as:

$$\mathbf{C}_{2RR} = \begin{bmatrix} C_{2RR,11} & 0 & C_{2RR,13} \\ 0 & C_{2RR,22} & 0 \\ C_{2RR,31} & 0 & C_{2RR,33} \end{bmatrix} \tag{7}$$

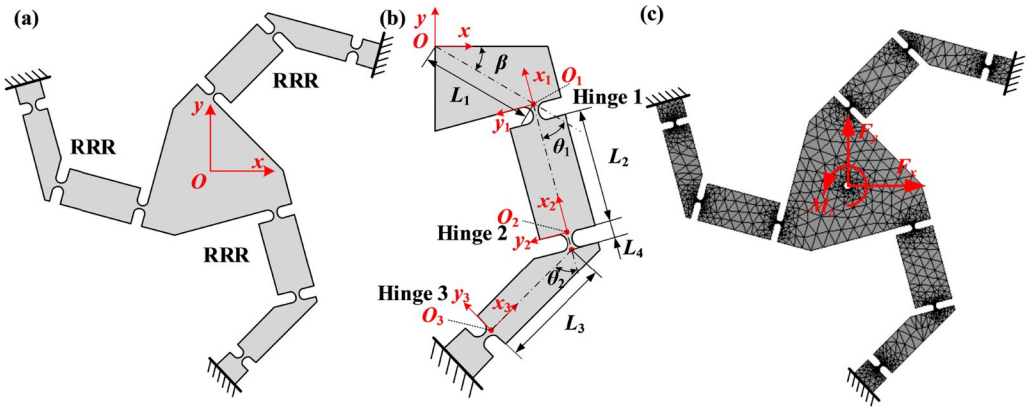

Fig. 4. (a) Schematic of 3RRR compliant mechanism; (b) coordinate and dimension definition of one limb of 3RRR compliant mechanism; (c) FEM model.

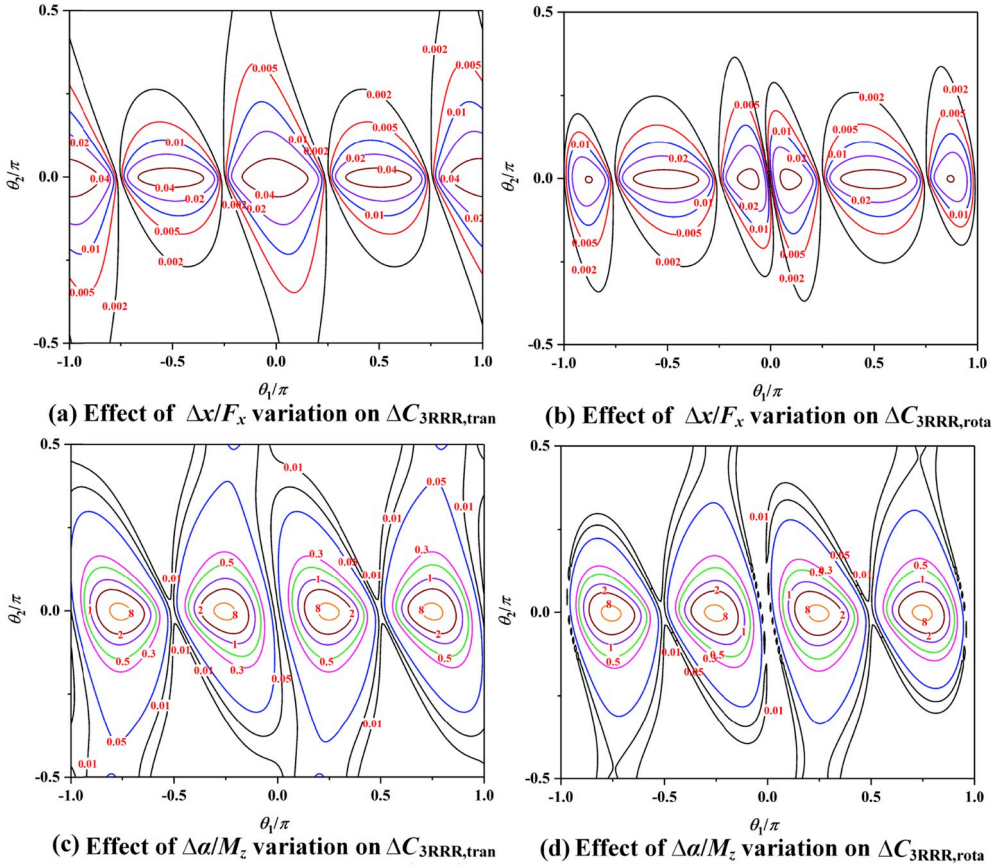

Fig. 5. Effects of compliance variation of RCFH on the output compliance variation of 3RRR compliant mechanism. The geometry parameters and material properties are set as follows: $E = 210$ GPa, $\nu = 0.3$, $\beta = 0$, $L_1 = L_2 = L_3 = 3$ mm, $L_4 = 2$ mm, $R = 1$ mm, $t = 0.5$ mm, and $b = 5$ mm (see Fig. 4 for 3RRR geometries).

Table 1
Calculation case (m/N, rad/N, rad/Nm) of 3RRR compliant mechanism when $t = 0.5$ mm, $R = 1$ mm, $b = 5$ mm, $\beta = 30°$, $L_1 = L_2 = L_3 = 20$ mm, $L_4 = 2$ mm.

Case	Chosen flexure hinge equation			Flexure hinge compliance		
	$\Delta x/F_x$	$\Delta y/F_y$	$\Delta\alpha/M_z$	$\Delta x/F_x$	$\Delta y/F_y$	$\Delta\alpha/M_z$
Case 1	Wu [20]	Wu [20]	Sch [22]	2.47×10^{-9}	8.52×10^{-8}	8.49×10^{-2}
Case 2	0	0	Sch [22]	0	0	8.49×10^{-2}

where $C_{2RR,ij}$ denotes the ith row and jth column element of the compliance matrix of 2RR mechanism. Detailed derivation of Eq. (7) is illustrated in Appendix C.2.

Fig. 7 shows the output compliance variation of 2RR mechanism resulting from the variation (5%) of $\Delta x/F_x$ and $\Delta\alpha/M_z$ when θ and L are varying. Fig. 7(a) and (b) are the surface plots of the effect of variation of translational compliance $\Delta x/F_x$ on the modeling accuracy of output compliance factors. The output compliance variations are bounded in the assessment range of different spatial configurations. While as shown in Fig. 7(c), the contour plot of compliance variance, the variation of $\Delta\alpha/M_z$ induces large numerical error in $C_{2RR,11}$, which exceeds 70% when $L \approx 4$ mm and $\theta > 0.4$. The validity of the matrix method for modeling 2RR compliant mechanism also depends on its spatial configuration, which is discussed as follows.

(1) Fig. 3(e) shows a general spatial configuration of 2RR mechanism where $\theta \neq 0$, which has only one rotational DOF. The rotational compliance of RCFH is dominant in the output rotational compliance of 2RR mechanism. On the other hand, neither the rotational or radial translational compliance of RCFH is dominant in the

Table 2
Calculation results (m/N, rad/N, rad/Nm) of 3RRR compliant mechanism.

Methods	$\theta_1 = 45°, \theta_2 = 60°$		$\theta_1 = 45°, \theta_2 = 30°$		$\theta_1 = 60°, \theta_2 = 60°$	
	C_{tran}	C_{rota}	C_{tran}	C_{rota}	C_{tran}	C_{rota}
FEM	3.57×10^{-6}	3.13×10^{-3}	1.04×10^{-6}	1.31×10^{-3}	3.58×10^{-6}	3.07×10^{-3}
Case 1	3.75×10^{-6}	3.46×10^{-3}	1.10×10^{-6}	1.41×10^{-3}	3.64×10^{-6}	3.40×10^{-3}
Difference to FEM	5.0%	10.5%	5.7%	7.6%	1.7%	10.7%
Case 2	3.71×10^{-6}	3.43×10^{-3}	1.08×10^{-6}	1.39×10^{-3}	3.57×10^{-6}	3.33×10^{-3}
Difference to FEM	3.9%	9.6%	3.8%	6.1%	−0.3%	8.5%

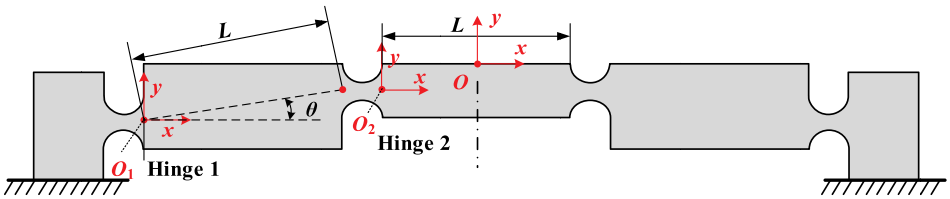

Fig. 6. Schematic and geometric configuration of 2RR compliant mechanism.

output translational compliance of 2RR mechanism. Hence the matrix method is only valid for calculating the output rotational compliance $C_{2RR,33}$, but invalid for the translational compliance $C_{2RR,11}$ when L/θ is small.

(2) Fig. 3(f) shows a specific spatial configuration of 2RR mechanism where $\theta = 0$, which is a singular configuration. But since the extended lines of two limbs are collinear, this spatial configuration has two DOFs including a rotational DOF (D_M) and a translational DOF (D_y). The rotational compliance of RCFH is dominant in the output compliances $C_{2RR,22}$ and $C_{2RR,33}$ of 2RR mechanism. Moreover, the radial translational compliance of RCFH is dominant in the output compliance of $C_{2RR,11}$ of 2RR mechanism. Hence as shown in Fig. 7, when $\theta = 0^{\circ}$, the relative variations of output compliance induced by the variation of $\Delta x/F_x$ or $\Delta\alpha/M_z$ are always small. It indicates that the matrix method is suitable in the output compliance modeling of 2RR compliant mechanism when $\theta = 0$. As to be noted, many researchers have successfully used CMM to model various 2RR mechanisms with $\theta = 0$ [10,13,14].

3.3. Bridge-type compliant mechanism

The spatial configuration of bridge-type mechanism is illustrated in Fig. 8. It consists of eight RCFHs. Based on CMM, the output compliance matrix $\mathbf{C}_{\text{bridge}}$ of bridge-type mechanism can be derived as:

$$\mathbf{C}_{\text{bridge}} = \begin{bmatrix} C_{\text{bridge},11} & 0 & C_{\text{bridge},13} \\ 0 & C_{\text{bridge},22} & 0 \\ C_{\text{bridge},31} & 0 & C_{\text{bridge},33} \end{bmatrix} \tag{8}$$

where $C_{\text{bridge},ij}$ denotes the ith row and jth column element of the compliance matrix of bridge-type mechanism respectively. Detailed derivation of Eq. (8) is illustrated in Appendix C.3.

Fig. 9 shows the surface plots of the output compliance variation of bridge-type mechanism induced by the variation of $\Delta x/F_x$ and $\Delta\alpha/M_z$ for different L and θ. The relative variations of output compliance of bridge-type mechanism are always bounded by 5% regardless the spatial configuration of the system. This is consistent with the predicted

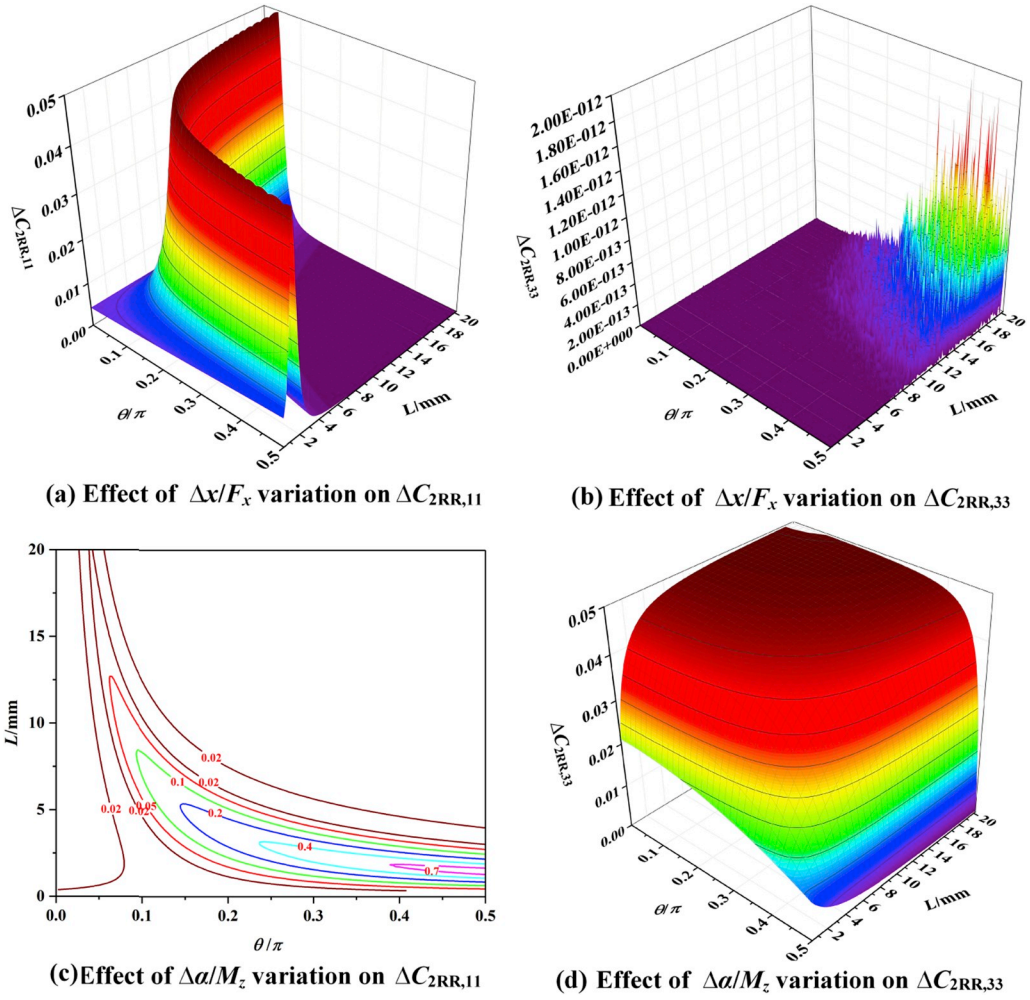

Fig. 7. Effects of compliance variation of RCFH on the output compliance variation of 2RR compliant mechanism.

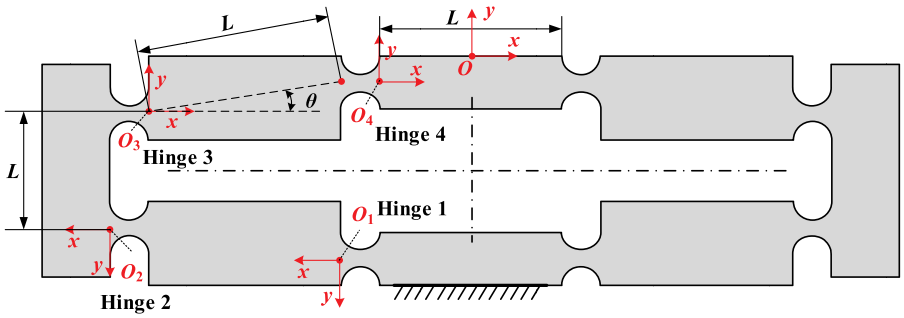

Fig. 8. Geometries of bridge-type compliant mechanism.

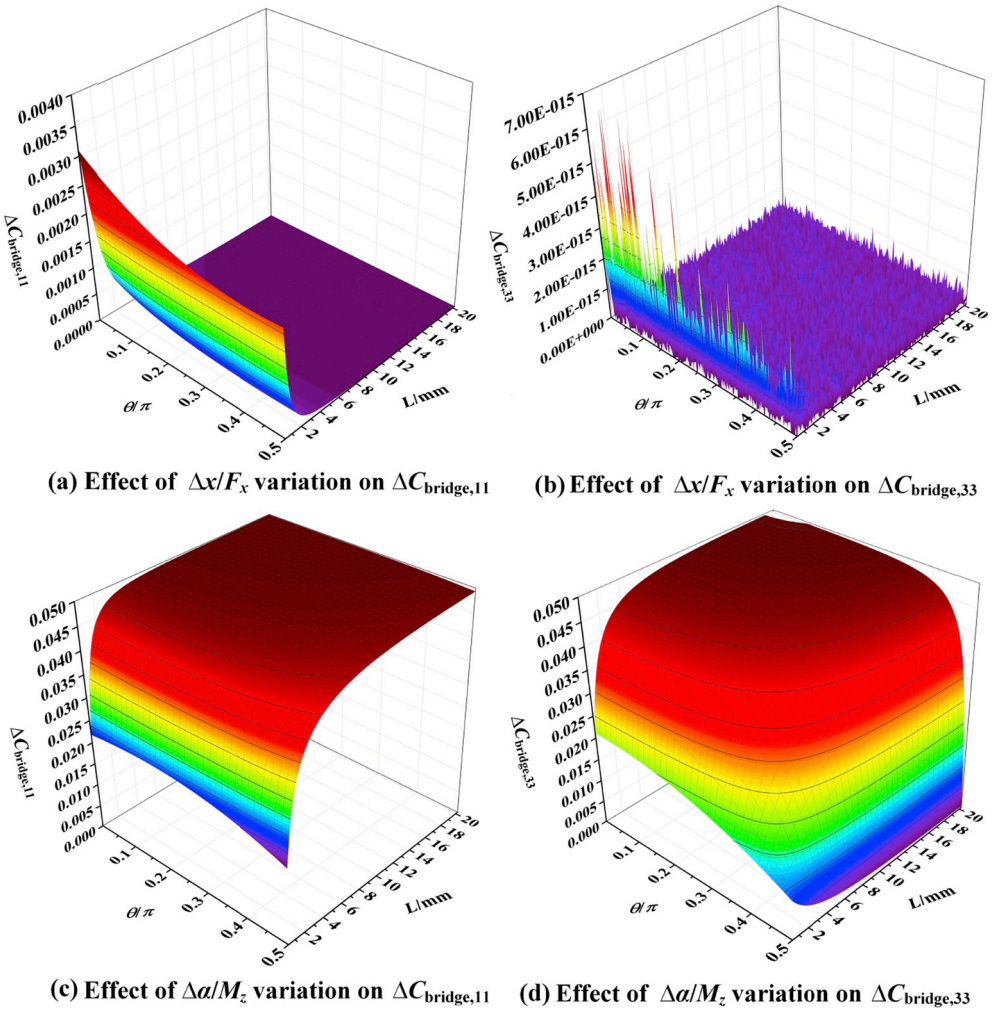

Fig. 9. Effects of compliance variation of RCFH on the output compliance variation of bridge-type mechanism.

results of DOF analysis. As shown in Fig. 3(g), the output platform of bridge-type mechanism has complete three DOFs even when $\theta = 0$ or $\pi/2$. The rotational compliance of RCFH is dominant in all the output compliances of bridge-type mechanism. Hence the matrix method is always valid for the output compliance modeling of bridge-type mechanism.

4. Conclusions

This study focuses on the validity evaluation of compliance-based matrix method (CMM) in the output compliance modeling of flexure-hinge mechanism. Planar 3RRR, 2RR and bridge-type mechanisms composed of right circular flexure-hinges (RCFHs) are selected for case studies. Based on the analyses above, the following conclusions can be drawn:

(1) The compliance matrix of RCFH expressed in its local frame is usually ill-conditioned due to the domination of rotational compliance factor. Inverse operation of the compliance matrix may result in numerical instability when calculating the stiffness matrix of RCFH.
(2) The validity of CMM is highly related to the mechanism type (serial or parallel), spatial configuration and singularity of the structure. For serial compliant mechanism, the calculation of output compliance does

not involve matrix inversion. The CMM can be effectively applied in calculating its output compliance with acceptable accuracy due to the linear superposition of RCFH compliances.

(3) For parallel compliant mechanism, the CMM is not always suitable for output compliance modeling due to the inevitable matrix inversion. A general criterion for the CMM validity is proposed as follows: if the radial translational compliance or the rotational compliance of RCFH is dominant in the output compliance of parallel mechanism, the matrix method is valid. By assuming that the RCFHs only have the rotational DOF, the DOF analysis is applied to help clarify the dominance of rotational compliance of RCFH under different spatial configurations. The predicted results of this criterion are consistent with the numerical evaluation on typical parallel compliant mechanisms including 3RRR, 2RR and bridge-type.

(4) The singularity of the spatial configuration does not always result in the invalidity of CMM. Even under a singular configuration, the CMM can still be valid if the translational or rotational compliance of RCFH is dominant in the overall output compliances of the parallel compliant mechanism.

Acknowledgements

The authors would like to acknowledge the support provided by the Innovation and Technology Fund, Hong Kong, grant #ITS/076/17; Shun Hing Institute of Advanced Engineering, The Chinese University of Hong Kong, # RNE-p4-17; and the start-up fund provided by McCormick School of Engineering, Northwestern University, Evanston, USA.

Appendix A. Compliance and stiffness equations of RCFH

The radial translational compliance of RCFH can be calculated by Ref. [20]:

$$\frac{\Delta x}{F_x} = \frac{1}{Eb}\left[\frac{2(2s+1)}{\sqrt{4s+1}}\arctan(\sqrt{4s+1}) - \frac{\pi}{2}\right] \tag{A.1}$$

where $s = R/t$. The tangential translational compliance of RCFH can be calculated by Ref. [20]:

$$\frac{\Delta y}{F_y} = \frac{12}{Eb}\left(\frac{s(24s^4+24s^3+22s^2+8s+1)}{2(2s+1)(4s+1)^2} + \frac{(2s+1)(24s^4+8s^3-14s^2-8s-1)}{2(4s+1)^{5/2}}\arctan(\sqrt{4s+1}) + \frac{\pi}{8}\right) + \frac{1}{Gb}\left[\frac{2(2s+1)}{\sqrt{4s+1}}\arctan(\sqrt{4s+1}) - \frac{\pi}{2}\right] \tag{A.2}$$

The rotational compliance of RCFH can be calculated by Ref. [22]:

$$\frac{\Delta\alpha}{M_z} = \left(\frac{Ebt^2}{12}\left[-0.0089 + 1.3556\sqrt{\frac{t}{2R}} - 0.5227\left(\sqrt{\frac{t}{2R}}\right)^2\right]\right)^{-1} \tag{A.3}$$

The stiffness factors of RCFH can be calculated by:

$$\begin{cases} K_{11} = \frac{1}{C_{11}} \\ K_{22} = \frac{1}{C_{22} - R^2 C_{33}} \\ K_{23} = K_{32} = -\frac{R}{C_{22} - R^2 C_{33}} \\ K_{33} = \frac{C_{22}}{C_{22}C_{33} - R^2 C_{33}^2} \end{cases} \tag{A.4}$$

Appendix B. General model of output compliance

As shown in Fig. 1, a local frame $x_iO_iy_i$ is attached to the RCFH. The compliance matrix $\mathbf{C}_{\mathrm{RCFH}}$ donates the relationship between loading $\mathbf{F} = [F_x, F_y, M_\alpha]^T$ and deformation $\boldsymbol{\delta} = [\Delta x, \Delta y, \Delta\alpha]^T$.

$$\boldsymbol{\delta} = \mathbf{C}_{\mathrm{RCFH}}\mathbf{F} \tag{B.1}$$

The serial compliant mechanism comprises several flexure hinges as shown in Fig. 1(a). The reference coordinate xOy is attached to the output platform. The compliance $\mathbf{C}_{\mathrm{RCFH}}$ can be transformed to the frame xOy by

$$\mathbf{C}_i^0 = \mathbf{T}_i^0 \mathbf{C}_{\mathrm{RCFH}} (\mathbf{T}_i^0)^{\mathrm{T}} \tag{B.2}$$

where the transformation matrix $\mathbf{T}_i$ takes the following form:

$$\mathbf{T}_i = \mathbf{T}(\alpha, \mathbf{r}) = \mathbf{T}(\alpha, (r_x, r_y)^{\mathrm{T}}) = \begin{bmatrix} \cos\alpha & \sin\alpha & r_y \\ -\sin\alpha & \cos\alpha & -r_x \\ 0 & 0 & 1 \end{bmatrix} \tag{B.3}$$

where α is the rotation angle of coordinate $x_iO_iy_i$ with respect to xOy, $\mathbf{r} = (r_x, r_y)^{\mathrm{T}}$ is the position vector of point O_i expressed in the reference frame O.

The compliance matrix $\mathbf{C}_{\mathrm{serial}}$ of serial mechanism is the summation of the compliances of individual RCFHs. It can be derived as:

$$\mathbf{C}_{\mathrm{serial}} = \sum \mathbf{C}_i^0 \tag{B.4}$$

The parallel compliant mechanism comprises several parallel limbs as shown in Fig. 1(b). The reference coordinate xOy of parallel compliant mechanism is also attached to its output platform or the end effector. The compliance matrix $\mathbf{C}_{\mathrm{limb},i}$ of limb i can be calculated through the method illustrated in Eq. (B.4). It can be transformed to the frame xOy:

$$\mathbf{C}^0_{\text{limb},i} = \mathbf{T}^0_i \mathbf{C}_{\text{limb},i} (\mathbf{T}^0_i)^{\mathrm{T}} \tag{B.5}$$

The compliance matrix $\mathbf{C}_{\text{parallel}}$ of parallel mechanism is the summation of the stiffness matrices (inverse of compliance) of all the limbs. It can be expressed as:

$$\mathbf{C}_{\text{parallel}} = \left(\sum (\mathbf{C}^0_{\text{limb},i})^{-1}\right)^{-1} \tag{B.6}$$

Appendix C. Output compliance derivation of typical compliant mechanisms

C.1. Output compliance matrix of 3RRR mechanism

In Fig. 4, the position vectors of point O_i expressed in the reference frame O are

$$\mathbf{r}_{1,3\text{RRR}} = (L_1 \cdot \cos(-\beta),\ L_1 \cdot \sin(-\beta))^{\mathrm{T}} \tag{C.1}$$

$$\mathbf{r}_{2,3\text{RRR}} = \mathbf{r}_1 + ((2R + L_2) \cdot \cos(-(\beta + \theta_1)),\ (2R + L_2) \cdot \sin(-(\beta + \theta_1)))^{\mathrm{T}} \tag{C.2}$$

$$\mathbf{r}'_{2,3\text{RRR}} = \mathbf{r}_1 + ((2R + L_2 + L_4) \cdot \cos(-(\beta + \theta_1)),\ (2R + L_2 + L_4) \cdot \sin(-(\beta + \theta_1)))^{\mathrm{T}} \tag{C.3}$$

$$\mathbf{r}_{3,3\text{RRR}} = \mathbf{r}'_{2,3\text{RRR}} + (L_3 \cdot \cos(-(\beta + \theta_1 + \theta_2)),\ L_3 \cdot \sin(-(\beta + \theta_1 + \theta_2)))^{\mathrm{T}} \tag{C.4}$$

The compliance matrices of hinge 1, hinge 2 and hinge 3 of 3RRR mechanism expressed in reference the frame O are

$$\mathbf{C}^0_{1,3\text{RRR}} = \mathbf{T}(\pi - \beta - \theta_1,\ \mathbf{r}_1) \cdot \mathbf{C}_{\text{RCFH}} \cdot \mathbf{T}(\pi - \beta - \theta_1,\ \mathbf{r}_1)^{\mathrm{T}} \tag{C.5}$$

$$\mathbf{C}^0_{2,3\text{RRR}} = \mathbf{T}(\pi - \beta - \theta_1,\ \mathbf{r}_2) \cdot \mathbf{C}_{\text{RCFH}} \cdot \mathbf{T}(\pi - \beta - \theta_1,\ \mathbf{r}_2)^{\mathrm{T}} \tag{C.6}$$

$$\mathbf{C}^0_{3,3\text{RRR}} = \mathbf{T}(\pi - \beta - \theta_1 - \theta_2,\ \mathbf{r}_3) \cdot \mathbf{C}_{\text{RCFH}} \cdot \mathbf{T}(\pi - \beta - \theta_1 - \theta_2,\ \mathbf{r}_3)^{\mathrm{T}} \tag{C.7}$$

The compliance matrix of limb 1 of 3RRR mechanism can be derived as:

$$\mathbf{C}_{\text{limb},1,3\text{RRR}} = \mathbf{C}^0_{1,3\text{RRR}} + \mathbf{C}^0_{2,3\text{RRR}} + \mathbf{C}^0_{3,3\text{RRR}} \tag{C.8}$$

Due to the symmetry of 3RRR mechanism, the compliance matrices of limb 2 and limb 3 can be calculated as:

$$\mathbf{C}^0_{\text{limb},2,3\text{RRR}} = \mathbf{T}\left(\frac{2\pi}{3},\ 0\right) \cdot \mathbf{C}^0_{\text{limb},1,3\text{RRR}} \cdot \mathbf{T}\left(\frac{2\pi}{3},\ 0\right)^{\mathrm{T}} \tag{C.9}$$

$$\mathbf{C}^0_{\text{limb},3,3\text{RRR}} = \mathbf{T}\left(-\frac{2\pi}{3},\ 0\right) \cdot \mathbf{C}^0_{\text{limb},1,3\text{RRR}} \cdot \mathbf{T}\left(-\frac{2\pi}{3},\ 0\right)^{\mathrm{T}} \tag{C.10}$$

Then the output compliance matrix of 3RRR can be derived as:

$$\mathbf{C}_{3\text{RRR}} = \left((\mathbf{C}^0_{\text{limb},1,3\text{RRR}})^{-1} + (\mathbf{C}^0_{\text{limb},2,3\text{RRR}})^{-1} + (\mathbf{C}^0_{\text{limb},3,3\text{RRR}})^{-1}\right)^{-1} \tag{C.11}$$

C.2. Output compliance matrix of 2RR mechanism

In, the position vectors of point O_i expressed in the reference frame O are

$$\mathbf{r}_{1,2\text{RR}} = -(0.5L + 2R + L\cos\theta,\ R + 0.5t + L\sin\theta)^{\mathrm{T}} \tag{C.12}$$

$$\mathbf{r}_{2,2\text{RR}} = -(0.5L,\ R + 0.5t)^{\mathrm{T}} \tag{C.13}$$

The compliance matrices of hinge 1, hinge 2 of 2RR mechanism expressed in the reference frame O are

$$\mathbf{C}^0_{1,2\text{RR}} = \mathbf{T}(0,\ \mathbf{r}_{1,2\text{RR}}) \cdot \mathbf{C}_{\text{RCFH}} \cdot \mathbf{T}(0,\ \mathbf{r}_{1,2\text{RR}})^{\mathrm{T}} \tag{C.14}$$

$$\mathbf{C}^0_{2,2\text{RR}} = \mathbf{T}(0,\ \mathbf{r}_{2,2\text{RR}}) \cdot \mathbf{C}_{\text{RCFH}} \cdot \mathbf{T}(0,\ \mathbf{r}_{2,2\text{RR}})^{\mathrm{T}} \tag{C.15}$$

The compliance matrix of left limb of 2RR mechanism can be derived as:

$$\mathbf{C}^0_{\text{limb,left},2\text{RR}} = \mathbf{C}^0_{1,2\text{RR}} + \mathbf{C}^0_{2,2\text{RR}} \tag{C.16}$$

Due to the symmetry of 2RR mechanism, the compliance of right limb can be calculated as:

$$\mathbf{C}^0_{\text{limb,right},2\text{RR}} = \mathbf{T}_y \mathbf{C}^0_{\text{limb,left},2\text{RR}} \mathbf{T}_y^{\mathrm{T}} \tag{C.17}$$

where $\mathbf{T}_y$ is the transformation matrix, it can be expressed as

$$\mathbf{T}_y = \begin{bmatrix} -1 & 0 & 0 \\ 0 & 1 & 0 \\ 0 & 0 & -1 \end{bmatrix} \tag{C.18}$$

Then the output compliance matrix of 2RR mechanism can be derived as:

$$\mathbf{C}^0_{\text{Bridge},2\text{RR}} = \left((\mathbf{C}^0_{\text{limb,left},2\text{RR}})^{-1} + (\mathbf{C}^0_{\text{limb,right},2\text{RR}})^{-1}\right)^{-1} \tag{C.19}$$

C.3. Output compliance matrix of bridge-type mechanism

In Fig. 8, the position vectors of point O_i expressed in the reference frame O of bridge type amplifier are:

$$\mathbf{r}_{1,\text{bridge}} = -(0.5L + 2R,\ R + 0.5t + 2L\sin\theta + L)^{\mathrm{T}} \tag{C.20}$$

$$\mathbf{r}_{2,\text{bridge}} = -(0.5L + 4R + L\cos\theta,\ R + 0.5t + L\sin\theta + L)^{\mathrm{T}} \tag{C.21}$$

$$\mathbf{r}_{3,\text{bridge}} = -(0.5L + 2R + L\cos\theta,\ R + 0.5t + L\sin\theta)^{\mathrm{T}} \tag{C.22}$$

$$\mathbf{r}_{4,\text{bridge}} = -(0.5L,\ R + 0.5t)^{\mathrm{T}} \tag{C.23}$$

The compliance matrices of hinge 1, hinge 2, hinge 3 and hinge 4 of bridge-type mechanism expressed in the reference frame O are

$$\mathbf{C}^0_{1,\text{bridge}} = \mathbf{T}(\pi,\ \mathbf{r}_1)\cdot\mathbf{C}_{\text{RCFH}}\cdot\mathbf{T}(\pi,\ \mathbf{r}_1)^{\mathrm{T}} \tag{C.24}$$

$$\mathbf{C}^0_{2,\text{bridge}} = \mathbf{T}(\pi,\ \mathbf{r}_{2,\text{bridge}})\cdot\mathbf{C}_{\text{RCFH}}\cdot\mathbf{T}(\pi,\ \mathbf{r}_{2,\text{bridge}})^{\mathrm{T}} \tag{C.25}$$

$$\mathbf{C}^0_{3,\text{bridge}} = \mathbf{T}(0,\ \mathbf{r}_{3,\text{bridge}})\cdot\mathbf{C}_{\text{RCFH}}\cdot\mathbf{T}(0,\ \mathbf{r}_{3,\text{bridge}})^{\mathrm{T}} \tag{C.26}$$

$$\mathbf{C}^0_{4,\text{bridge}} = \mathbf{T}(0,\ \mathbf{r}_{4,\text{bridge}})\cdot\mathbf{C}_{\text{RCFH}}\cdot\mathbf{T}(0,\ \mathbf{r}_{4,\text{bridge}})^{\mathrm{T}} \tag{C.27}$$

The compliance matrix of left limb of bridge-type mechanism can be derived as:

$$\mathbf{C}^0_{\text{limb,left,bridge}} = \mathbf{C}^0_{1,\text{bridge}} + \mathbf{C}^0_{2,\text{bridge}} + \mathbf{C}^0_{3,\text{bridge}} + \mathbf{C}^0_{4,\text{bridge}} \tag{C.28}$$

Due to the symmetry of bridge-type mechanism, the compliance matrix of right limb can be calculated as:

$$\mathbf{C}^0_{\text{limb,right,bridge}} = \mathbf{T}_y\mathbf{C}^0_{\text{limb,left,bridge}}\mathbf{T}_y^{\mathrm{T}} \tag{C.29}$$

Then the output compliance matrix of bridge-type mechanism can be derived as:

$$\mathbf{C}_{\text{Bridge}} = ((\mathbf{C}^0_{\text{limb,left,bridge}})^{-1} + (\mathbf{C}^0_{\text{limb,right,bridge}})^{-1})^{-1} \tag{C.30}$$

Appendix D. Supplementary data

Supplementary data to this article can be found online at https://doi.org/10.1016/j.precisioneng.2019.02.006.

References

[1] Wu Z, Xu Q. Survey on recent designs of compliant micro-/nano-positioning stages. Actuators 2018;7(1):5.
[2] Zhu W, Zhu Z, He Y, Ehmann KF, Ju B, Li S. Development of a novel 2-d vibration-assisted compliant cutting system for surface texturing. IEEE/ASME Trans Mecha 2017;22(4):1796–806.
[3] Chen K, Si C, Guo P. Design of a high bandwidth non-resonant tertiary motion generator for elliptical vibration texturing. J Micro Nano Manuf 2017;5(1):11008.
[4] Jia X, Liu J, Tian Y, Zhang D. Stiffness analysis of a compliant precision positioning stage. Robotica 2012;30(06):925–39.
[5] Jiang Y, Li TM, Wang LP. Stiffness modeling of compliant parallel mechanisms and applications in the performance analysis of a decoupled parallel compliant stage. Rev Sci Instrum 2015;86(9):95109.
[6] Yong YK, Lu T. The effect of the accuracies of flexure hinge equations on the output compliances of planar micro-motion stages. Mech Mach Theor 2008;43(3):347–63.
[7] Pham H, Chen I. Stiffness modeling of flexure parallel mechanism. Precis Eng 2005;29(4):467–78.
[8] Howell LL, Midha A, Norton TW. Evaluation of equivalent spring stiffness for use in a pseudo-rigid-body model of large-deflection compliant mechanisms. J Mech Des 1996;118(1):126–31.
[9] Aydın YO, Galloway KC, Yazicioglu Y, Koditschek DE. Modeling the compliance of a variable stiffness c-shaped leg using castigliano's theorem. ASME 2010 international design engineering technical conferences and computers and information in engineering conference. 2010. p. 705–13.
[10] Li Y, Xu Q. Design and analysis of a totally decoupled flexure-based xy parallel micro-manipulator. IEEE Trans Robot 2009;25(3):645–57.
[11] Choi K, Lee JJ. Static model for flexure-based compliant mechanism driven by piezo stacks. Proc Inst Mech Eng C-J Mech Eng Sci 2008;222(4):703–9.
[12] Lobontiu N. Compliance-based matrix method for modeling the quasi-static response of planar serial flexure-hinge mechanisms. Precis Eng 2014;38(3):639–50.
[13] Zhu Z, To S, Zhu W, Li Y, Huang P. Optimum design of a piezo-actuated tri-axial compliant mechanism for nano-cutting. IEEE Trans Ind Electron 2018;65(8):6362–71.
[14] Zhu Z, Zhou X, Liu Z, Wang R, Zhu L. Development of a piezo-electrically actuated two-degree-of-freedom fast tool servo with decoupled motions for micro-/nano-machining. Precis Eng 2014;38(4):809–20.
[15] Yong YK, Lu T, Handley DC. Review of circular flexure hinge design equations and derivation of empirical formulations. Precis Eng 2008;32(2):63–70.
[16] Tseytlin YM. Notch flexure hinges: an effective theory. Rev Sci Instrum 2002;73(9):3363–8.
[17] Lobontiu N, Paine JS, Garcia E, Goldfarb M. Design of symmetric conic-section flexure hinges based on closed-form compliance equations. Mech Mach Theor 2002;37(5):477–98.
[18] Paros JM. How to design flexure hinges. Mach Des 1965;37:151–6.
[19] Lobontiu N. Compliant mechanisms: design of flexure hinges. CRC press; 2002.
[20] Wu Y, Zhou Z. Design calculations for flexure hinges. Rev Sci Instrum 2002;73(8):3101–6.
[21] Smith ST, Chetwynd DG, Bowen DK. Design and assessment of monolithic high precision translation mechanisms. J Phys E Sci Instrum 1987;20(8):977.
[22] Schotborgh WO, Kokkeler FG, Tragter H, van Houten FJ. Dimensionless design graphs for flexure elements and a comparison between three flexure elements. Precis Eng 2005;29(1):41–7.
[23] Ortega JM. Numerical analysis: a second course. SIAM; 1990.
[24] Chen G, Liu X, Gao H, Jia J. A generalized model for conic flexure hinges. Rev Sci Instrum 2009;80(5):055106.
[25] Chen G, Liu X, Du Y. Elliptical-arc-fillet flexure hinges: toward a generalized model for commonly used flexure hinges. J Mech Des 2011;133(8):081002.
[26] Liu X, Wang J. Parallel kinematics, type, kinematics, and optimal design. Berlin Heidelberg: Springer-Verlag; 2014.